Proceedings of 12th IOE Graduate Conference
Peer Reviewed
ISSN: 2350-8914 (Online), 2350-8906 (Print)
Year: 2022 Month: October Volume: 12

Numerical Study on Geogrid-Reinforced Flexible Pavement Sections

Arjun Poudel [a], Ram Chandra Tiwari [b]

[a, b] *Department of Civil Engineering, Pulchowk Campus, IOE, Tribhuvan University, Nepal*
[a] arjun.pdl27@gmail.com, [b] rct2075ce_rctiwari@pcampus.edu.np

Abstract
Environmental and traffic factors cause premature and severe damage to the flexible pavement, which incurs high maintenance costs. Geogrid can be introduced into the pavement layers to overcome the damage. The effectiveness of geogrid, in reducing surface displacement and subgrade strain level, as a reinforcement in a flexible pavement system has been investigated under this topic by numerical modelling using FEM-based software ”PLAXIS 3D”. The unreinforced pavement considered in this study is a 175 mm gravel base lying on a subgrade with a CBR of 5%. The biaxial geogrid of normal elastic stiffness 1000 kN/m was used to reinforce the pavement. Geogrid was sandwiched, at only one position at a time, at 25%, 50%, 75%, and 100% of the base thickness from the pavement surface. Static and moving traffic load on the pavement was simulated as dual point load assembly on each side of a standard axle of 80 kN. Varying the pavement thickness, geogrid stiffness, uniform acceleration and initial velocity of the standard axle, the effect on surface displacement and vertical compressive strain were reasonably analyzed. With this analysis, it is inferred that the inclusion of geogrid in the pavement reduces the surface displacement and vertical compressive strain level at the top of the subgrade of the flexible pavement system.

Keywords
Flexible Pavement, Geogrid, Finite Element Method, Vertical Compressive Strain, Moving Load

1. Introduction

In flexible pavement, the intensity of a load diminishes in geometrical proportion as it is transmitted downward from the surface, through successive layers of granular material, by spreading over an increasingly larger area [1]. The basic design principle of flexible pavement is based on layered system with better and more robust materials at the top, where the stress level is high, and weak and inferior materials at the bottom, where the stress level is low [2].

1.1 Problem Statement

When soft subgrade sites are encountered during the design and construction of flexible pavement, the prevailing solution for subgrade strengthening is mechanical stabilization or stabilization by using additives or replacing the weak subgrade with firmer soil that meets the desired specification. However, cost and quality control are other issues for the abovementioned solutions [1]. These types of weak subgrade issues encountered during the design and construction of flexible pavement can be addressed by introducing geogrid into the pavement layers [3].The geogrid introduced into pavement courses functions more or less in the same way as steel bars in reinforced concrete [3, 4].

Road traffic moves at varying velocities, with a specific value of acceleration and deacceleration. However, road designers have been using pavement design guidelines that still assume static traffic load to compute strain values at critical points. These strain values significantly differ when the pavement is loaded by moving axle load [5]. This difference in strain values hinders the realistic and economical design of the pavement, which can be addressed by considering the moving traffic load for the analysis followed by the design of pavement sections.

1.2 Objective

Regarding the general objective, this paper compares the effect of moving axle load with the static axle load

on the unreinforced and geogrid-reinforced flexible pavement. The specific objective set out for this study are:

1. To find out the optimum location of the geogrid in the low volume flexible pavement section,
2. To determine the most effective base thickness for geogrid reinforcement, and
3. To compare the vertical compressive strain at the top of the subgrade for static and moving axle load conditions in unreinforced and geogrid reinforced pavement sections.

1.3 Limitation

The Finite Element(FE) model is developed in such a way that it closely represents the actual site conditions. But because of constraints in the scope and methodology of this study, it has the following distinctive limitations.

1. Dual point load assembly on each side of the standard axle has been considered,
2. The dimension of the geogrid opening has not been not considered in this study.

2. Literature Review

In a flexible pavement system, points "H" and "V", as illustrated in Figure 1, are considered as critical points where horizontal tensile strain and vertical compressive strain will be maximum, respectively. The pavement thickness is so designed that the compressive stress on top of the subgrade is kept within its bearing capacity, and horizontal tensile stress on the bottom bituminous layer is kept within its flexural strength [6].

When very soft subgrade soil is encountered during the design, the designer shall have to provide very thick pavement layers to limit the stress levels within a permissible range which might be relatively more costly. So, reinforcing elements like geogrid can be introduced into the pavement to spread the traffic load in such a way that the stress levels at the top of the subgrade would be dramatically low and within its bearing capacity as portrayed in Figure 2 [7]. The end product is called reinforced pavement and has been widely used to stabilize road sub-base and subgrade, separate pavement layers, and mitigate reflective cracking in the bituminous layer since three decades [3]. The stress and strain parameters like plastic displacement of subgrade, vertical compressive stress at the top of subgrade, horizontal tensile strain under the bottom bituminous layer, and the rate of plastic displacement can be substantially reduced with the strengthening of flexible pavement with geogrid [7].

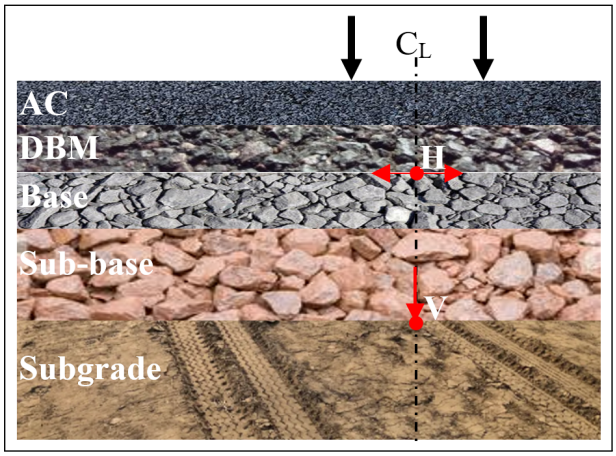

Figure 1: Critical points in a flexible pavement section with unbound base/sub-base materials

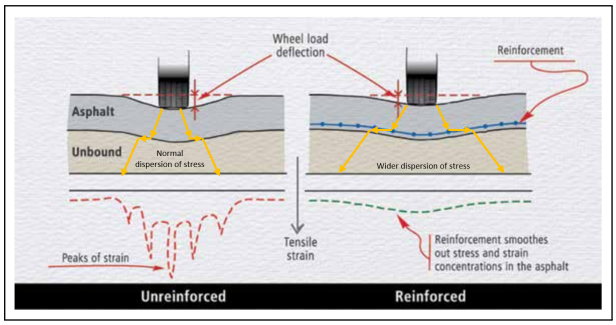

Figure 2: Stress distribution and reinforcement action in unreinforced and geogrid reinforced pavement section (Source: IRC SP 59 2019)

Geogrid is a geosynthetic material consisting of inter-connected sets of tensile elements forming rectangular or triangular apertures. The apertures in the geogrid allow the interlocking of material within, increasing the shear strength of the overlying material. Lateral restraint, bearing capacity increment, and tension membrane effect are the mechanisms in the geogrid reinforced pavement [4].

S. W. Perkins [8] concluded that notable enhancement in pavement performance as surface rutting was observed significantly for weak subgrade (CBR 1.5%) but slight improvement for stiffer subgrade (CBR 20%). Further, reinforcement provides at least a 20% reduction in aggregate base thickness. Large scale field test conducted by Al-Qadi et al. [9]

recommended that reinforcement placed at the base-subgrade interface will be effective for the thinner base. Further, they concluded that with an increase in base thickness, the efficiency of reinforcement to reduce surface displacement drops.

Nader & Sharbaf [4] introduced light duty biaxial and triaxial geogrid at mid-depth of thick aggregate base and subgrade/base interface of the thin base into the pavement and inferred that the vertical pressure at the center of the base-subgrade interface decreased by an average of 18 and 24% for biaxial and triaxial geogrid-reinforced sections, respectively. To investigate the load spreading capacity of geogrid reinforced pavement, Leng & Gabr [10] conducted a cyclic loading experiment on a clay-sand subgrade with base thicknesses of 15cm and 25cm, introducing the biaxial geogrid in the base-subgrade interface and concluding that the load spreading capacity of the reinforced pavement increases with the increase in stiffness or modulus of geogrid.

Meanwhile, Wu et al. [5] developed 2.5-D FE method to examine the viscoelastic pavement response on different four bituminous pavement sections under moving load condition and inferred that the pavement strain responses decreased as the speed of load increased due to viscoelastic behavior of bituminous course. Further, Ling & Liu [11] performed a laboratory test to study the benefit of geogrid reinforcement placed between the AC layer and Ottawa sand subgrade and inferred that the enhancement was more notable for dynamic than static loading.

3. Methodology

3.1 Data Collection

The flexible pavement considered in this study lies on a subgrade, with a california bearing ratio (CBR) of 5% and the total number of equivalent single axle load repetitions to be sustained by the pavement is 10000. In accordance with the flexible pavement design guidelines for low-volume roads (IRC SP 72 2015), the recommended unreinforced pavement section comprises only 175 mm of gravel base of CBR, not less than 80%. From laboratory tests, the bulk unit weight of subgrade soil and the base was found to be 18.2 and 22.27 kN/m3, respectively, and the CBR of the base was 88.65%. The axle load configuration considered in this study was dual point load assembly on each side of a 80 kN standard axle as shown in Figure 3.

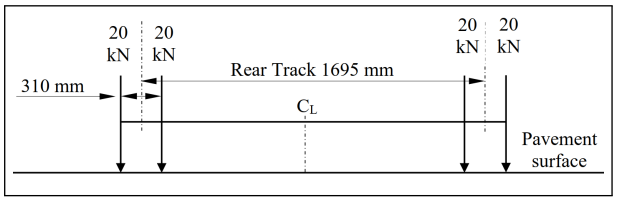

Figure 3: Schematic diagram for 80 kN standard axle load

Biaxial geogrid was introduced at 25% of the base thickness from the pavement surface to reinforce the unreinforced pavement. The tensile strength of geogrid was 25 kN/m in both directions, and the corresponding strain at maximum load was 2.5%. These values were referenced from the technical specification provided by Maccaferri Nepal Pvt. Ltd.

3.2 Finite element modelling

FEM-based software "PLAXIS 3D" was used to model the pavement section. The linear elastic model was assigned to simulate the subgrade and base. The model involves two elastic stiffness parameters: Young's modulus (E) and Poisson's ratio (ν). According to the Guidelines for the Design of Flexible Pavements (IRC 37 2018), the value of E for subgrade and base was computed as 50,000 kPa, and 102,180 kPa using Equation 1 and 2, respectively, and Poisson's ratio of 0.35 was taken for both subgrade and base as per above-mentioned guidelines.

Geogrid was simulated using an elastic model involving the normal elastic stiffness as an input parameter which was computed as 1000 kN/m using Equation 3. Tensile strength reduction factors for installation damage, creep, and degradation was not considered during the computation of normal elastic stiffness of geogrid.

$$E_{subgrade} = 10.0 * CBR_{subgrade} \tag{1}$$

where, $E_{subgrade}$ and $CBR_{subgrade}$ are the Young's modulus (kN/m^2) and CBR(%) of subgrade soil.

$$E_{base} = 0.2 * (h_{base})^{0.45} * E_{subgrade} \tag{2}$$

where, E_{base} and h_{base} are the Young's modulus (kN/m^2) and height of base (mm).

$$EA = \frac{T_{@\varepsilon\%}}{\varepsilon\%} \tag{3}$$

where, EA is normal elastic stiffness of the geogrid (kN/m), $T_{@\varepsilon\%}$ is tensile strength of the geogrid (kN/m), and $\varepsilon\%$ is the normal strain at maximum load.

Mainly for moving load conditions (dynamic analysis), the larger the model's geometry, the higher the calculation time. So, to optimize the model's geometry and computational time, the total dimension of the model was chosen as 20 m in length, 8 m and 23 m in the top and bottom width, and 5m in depth, as shown in Figure 4. The vertical stress change in the vicinity of the boundary in the negative z-direction was only 0.41% of maximum stress on the top of the pavement.

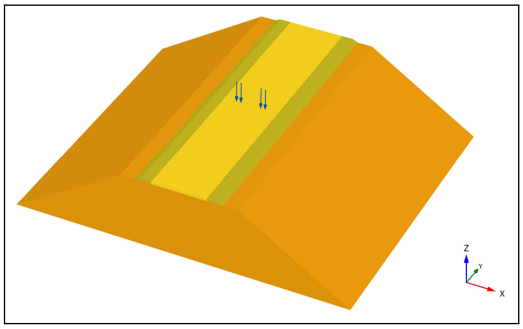

Figure 4: Geometric model of 175 mm pavement section in PLAXIS 3D

The meshing was done by assigning the values as illustrated in Table 1. Ten-noded tetrahedral elements were generated for soil material, whereas six-noded surface elements were generated for geogrid as depicted in Figure 5. As per this setting, an element's target element dimension and minimum sizes were 1.5443 m and 0.154 m, respectively.

Table 1: Value assigned for mesh generation

Mesh option	Value
Element distribution	Medium
Global scale factor	1.2
Minimum element size factor	0.005

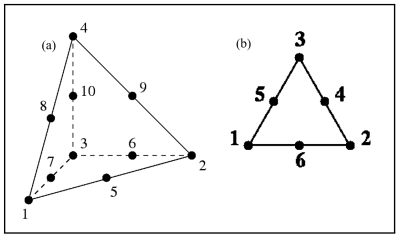

Figure 5: (a): 10 noded soil element and (b): 6 noded geogrid element (Source: Bentley)

The base and geogrid were locally refined with a coarseness factor of 0.3, except that at the central (3.75 m x 4 m x 0.175 m) portion, the coarseness factor was set to 0.1. In contrast, the shoulder and subgrade had a coarseness factor of 1.0, except that at the central (8 m x 4 m x 2 m) portion, the coarseness factor was set to 0.4. Further, the point load was locally refined with a coarseness factor of 0.1. FE-model after mesh generation and the quality of generated mesh in terms of signed inverse condition number (SICN) are illustrated in Figure 6 and Figure 7, respectively.

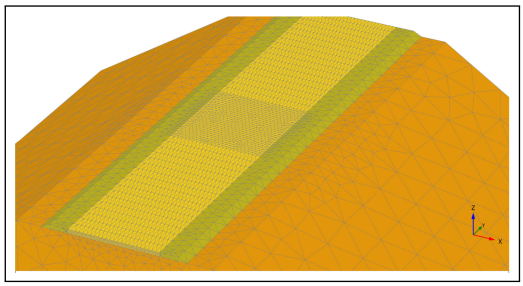

Figure 6: FE-model of 175 mm pavement section after mesh generation

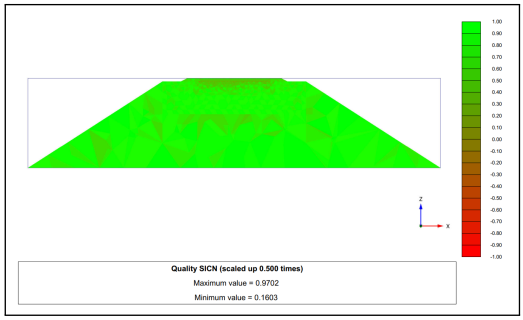

Figure 7: Quality of generated mesh in terms of SICN

3.3 Analysis of FE-model

Table 2: Dynamic parameters and assigned value

Parameter	Value
Axle movement along	Y-axis
Movement length (m)	1.0
Uniform acceleration of axle load (m/s^2)	0.00
Velocity of the axle (kmph)	5
Dynamic time (sec)	0.72
Maximum steps to store	100

Plastic and dynamic analyses were performed for static and moving axle load conditions, respectively. Parameters assigned during dynamic calculation are

illustrated in Table 2. Further analysis was performed by varying the base thickness, position and stiffness of geogrid, and uniform acceleration and velocity of axle load. Values taken for the parametric study are illustrated in Table 3.

Table 3: Parametric variation

Parameter	Value
Base thickness (mm)	175, 250, 325
Position of geogrid (%)	25, 50, 75, 100
Geogrid stiffness (kN/m)	1000, 3000, 5000
Acceleration (m/s^2)	0.0, 0.50, 0.75, 1.0
Velocity (kmph)	5 to 40, interval @ 5

4. Results and discussion

4.1 Effect of base thickness

Upon static loading on the unreinforced pavement, total displacement on the pavement surface (u_{sur}) and vertical compressive strain at the top of the subgrade under the center of a dual wheel (ε_{zz}) for a 175 mm base are found to be 3.785 mm, and 1.086E-3, respectively.

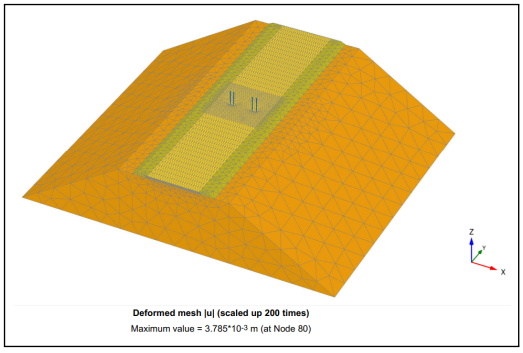

Figure 8: Deformed mesh of unreinforced 175 mm pavement section model

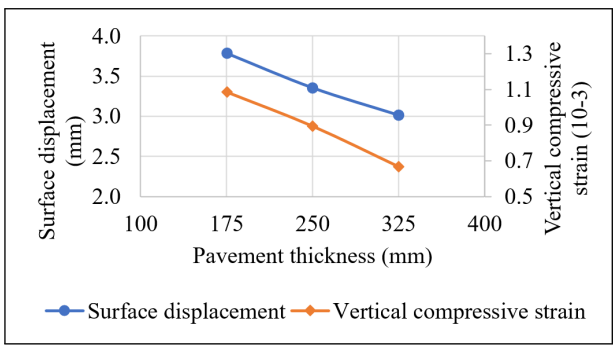

Figure 9: Variation of Surface displacement and vertical compressive strain with respect to base thickness

Deformed mesh obtained after numerical analysis for 175 mm pavement model is shown in Figure 8. Upon changing the base thickness by 75mm and 150 mm, u_{sur} reduced by 11% and 20%, respectively, whereas ε_{zz} decreased by 18% and 39%, respectively. Figure 9 shows the effect of base thickness on u_{sur} and ε_{zz}.

4.2 Effect of geogrid position

The effect of geogrid position on flexible pavement loaded by the standard axle under static conditions was examined by introducing geogrid of normal elastic stiffness 1000 kN/m at either 25%, 50%, 75%, or 100% of the base thickness, from the pavement surface.

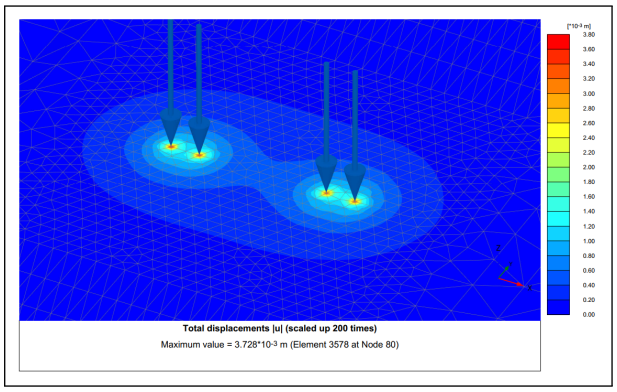

Figure 10: Total displacement shading for 175mm pavement reinforced at 25% of base thickness

Upon reinforcing a 175 mm base at 25% of base thickness from the pavement surface, u_{sur} and ε_{zz} were reduced by 1.51% and 1.75%, respectively. Analysis was repeated for another three positions of geogrid. The percentage reduction in u_{sur} decreased from 1.51% to 1.29%, 1.19%, and 1.22% when geogrid was introduced at 50%, 75%, and 100% of the base thickness, respectively as illustrated in Figure 12. Total displacement shading obtained from PLAXIS 3D for 175mm pavement reinforced at 25% of base thickness is shown in Figure 11.

However, with the downward positioning of geogrid from 25% to 100% of the base thickness at an interval of 25%, the % reduction in ε_{zz} increased from 1.75% to 2.21%, 3.25%, and 4.70%, respectively, as depicted in Figure 12.

This analysis was repeated for other pavement thicknesses of 250 mm and 325 mm. Upon positioning the geogrid at 25% of the base thickness, the percentage reduction in u_{sur} was found to be 1.51%, 1.04%, and 0.76% for 175 mm, 250 mm, and 325 mm pavement, respectively, as shown in Figure

11. Similarly, upon positioning the geogrid at 100% of the base thickness, the percentage reduction in ε_{zz} was found to be 4.70%, 3.36%, and 2.84% for 175 mm, 250 mm, and 325 mm pavement, respectively as illustrated in Figure 12.

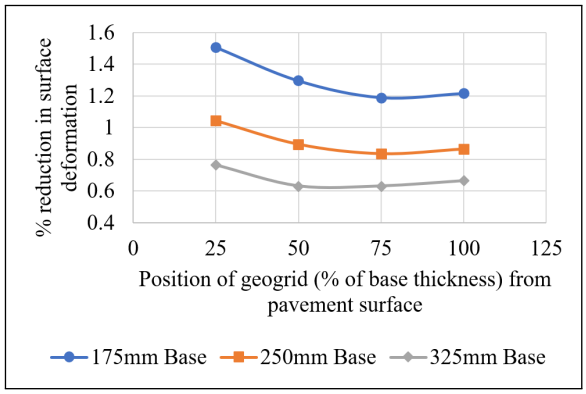

Figure 11: % reduction in surface displacement vs. position of geogrid of stiffness 1000 kN/m

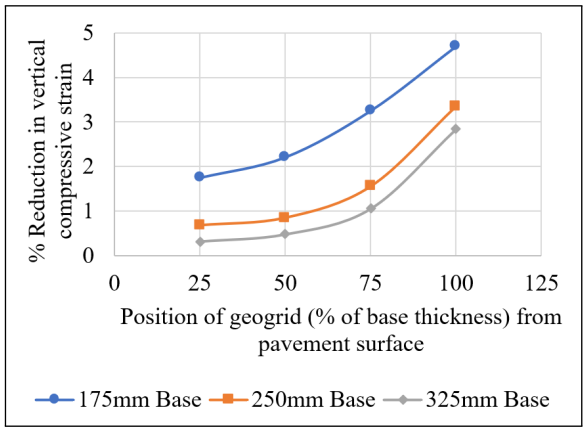

Figure 12: % reduction in the vertical compressive strain at the top of subgrade vs. position of geogrid of stiffness 1000 kN/m

The axial force (AF) and shear force (SF) induced in the geogrid were also examined with respect to the position of the geogrid and the base thickness. As depicted in Figure 14, maximum axial and shear force of magnitude 3.53 kN/m and 1.56 kN/m was pronounced when the geogrid was placed at 25% of the 175mm base. These magnitudes of axial and shear force decreased with an increase in base thickness or with the downward positioning of geogrid. A sample output from PLAXIS 3D for the axial force in geogrid introduced at 25% of 175mm base is illustrated in Figure 13.

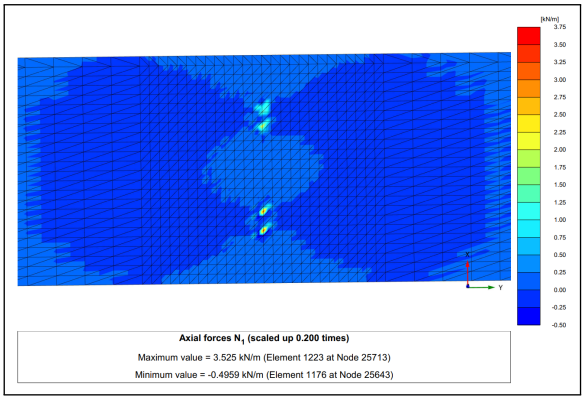

Figure 13: Shading for axial force in geogrid introduced at 25% of base thickness of 175mm pavement

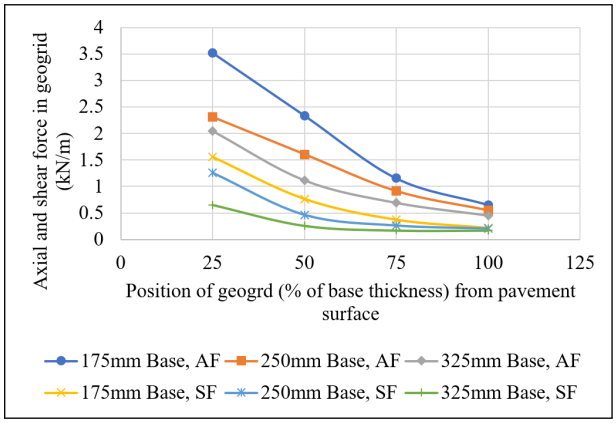

Figure 14: Axial and shear force in geogrid vs. position of geogrid of stiffness 1000 kN/m

4.3 Effect of geogrid stiffness

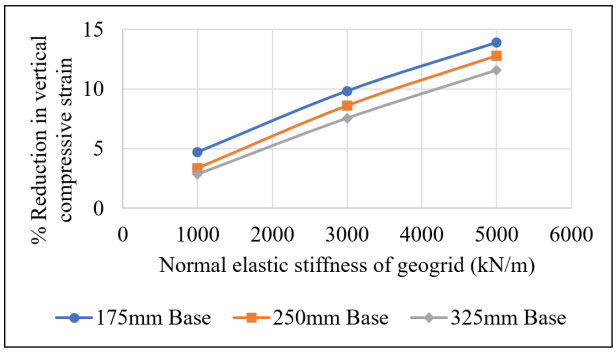

Figure 15: % reduction in the vertical compressive strain at the top of subgrade vs. stiffness of geogrid placed at the base-subgrade interface

Similarly, to analyze the effect of normal elastic stiffness of geogrid on ε_{zz}, geogrid of varying stiffness, as mentioned in Table 3, was introduced into the base-subgrade interface. Upon changing the

geogrid stiffness from 1000 to 3000 and then to 5000 kN/m, the percentage reduction in ε_{zz} was found to be 9.83% and 13.9%, respectively. In other words, on changing the geogrid stiffness to 3000 and 5000 kN/m, the % reduction in ε_{zz} was increased by a factor of approximately 2 and 3, respectively. The effect of increasing geogrid stiffness on ε_{zz} has been presented graphically in Figure 15. It was also observed that the % reduction in ε_{zz} increased with an increase in geogrid stiffness for 250 mm and 325 mm pavement sections considered in this study.

4.4 Effect of moving axle load

To examine the effect of moving axle load in terms of ε_{zz}, unreinforced pavement sections (URS) and geogrid-reinforced pavement sections (GRS) models were analyzed under static and moving axle load conditions. The movement of axle load on the FE-model was assigned in terms of movement distance, uniform acceleration, and the velocity of axle load as mentioned in Table 3. After numerical analysis, output values of ε_{zz} were extracted, and the graphical plot is illustrated Figure 16 with solid lines.

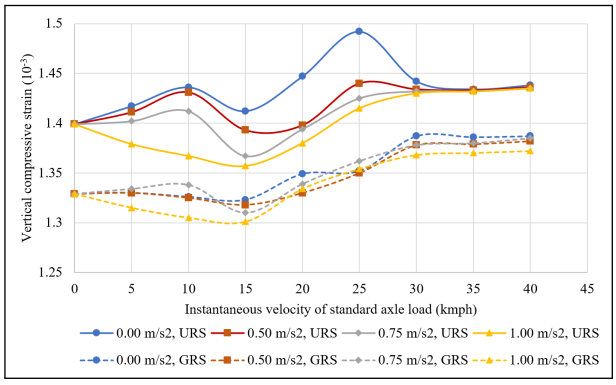

Figure 16: Variation of ε_{zz} with uniform acceleration and instantaneous velocity for unreinforced and reinforced pavement sections

At first, the implication of increasing uniform velocity (zero acceleration) on ε_{zz} was analyzed in the unreinforced section. When the initial velocity was assigned as 5 and 10 kmph, the ε_{zz} increased slightly by only 1.29% and 2.64%, respectively, with respect to that at static conditions. Further changing the uniform velocity to 15 kmph, the % increase in ε_{zz} reduced to only 0.93%. However, further changing the uniform velocity to 20 and 25 kmph, ε_{zz} again increased by 3.43% and 6.65%, respectively. Further changing the uniform velocity to 30, 35, and 40 kmph, the % increase in ε_{zz} dropped to 3.07%, 2.50%, and 2.79%, respectively as portrayed by solid lines in Figure 16.

When the uniform acceleration of 0.5 m/s^2 was assigned, the ε_{zz} at each instantaneous velocity was found to be smaller than that measured at zero acceleration. And, the similar pattern was observed for higher values of uniform acceleration upto 1 m/s^2. Irrespective of the uniform acceleration and instantaneous velocity of axle load, the maximum and minimum percentage increase in ε_{zz} was pronounced at the instantaneous velocity of 25 and 15 kmph, respectively. Furthermore, the effect of increasing uniform acceleration was noticeable for velocities ranging from 0 to 30 kmph.

The effect of geogrid reinforcement on pavement loaded with moving axle load was analyzed with the introduction of geogrid of normal elastic stiffness 1000 KN/m at the 175 mm base-subgrade interface. When axle load moved uniformly on the reinforced pavement, the % reduction in ε_{zz} increased up to 30 kmph as illustrated in Figure 17. Upon assigning the higher acceleration values, the % reduction in ε_{zz} decreased with respect to that computed for uniformly moving axle load. The maximum % reduction was achieved, as high as 9.4% and 6.3%, at the velocity of 25 kmph for the uniform acceleration of 0.00 and 0.50 m/s^2. These maximum % reduction in ε_{zz} values are about 2.00 and 1.35 times larger than that computed for static load conditions, respectively. However, for the constant acceleration of 0.75 and 1.00 m/s^2, the % reduction in ε_{zz} was even lower than that computed for the static condition. Furthermore, for velocities ranging from 30 to 40 kmph, irrespective of the acceleration of axle load, the % reduction in ε_{zz} was found to be smaller than that calculated for static conditions.

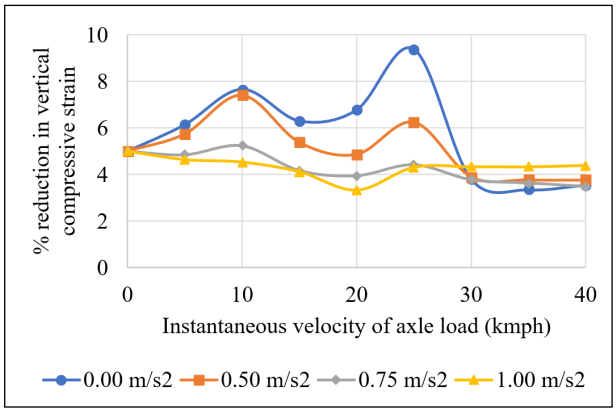

Figure 17: % change in ε_{zz} vs. instantaneous velocity of the standard axle for varying acceleration

5. Conclusion

A couple of FEM-based numerical model was generated varying the parameters as illustrated in Table 3 and analyzed to study the behaviour of unreinforced and geogrid reinforced flexible pavement sections upon static and moving axle conditions, and the following conclusions are drawn:

1. The effectiveness of geogrid reinforcement in lessening total displacement on the pavement surface (u_{sur}) and vertical compressive strain at the top of the subgrade under the center of a dual wheel (ε_{zz}) is more pronounced for the smaller pavement thickness.
2. Maximum percentage reduction in u_{sur} and ε_{zz} can be achieved by introducing geogrid at the 25% and 100% of the base thickness, respectively. These % reduction values increase with an increase in geogrid stiffness.
3. ε_{zz}, and axial and shear force in geogrid decline either with an increase in pavement thickness or with the downward positioning of the geogrid in the base course. Axial and shear force induced in geogrid ribs increase with an increase in geogrid stiffness.
4. Irrespective of the uniform acceleration of axle load, the maximum and minimum percentage increase in ε_{zz} due to moving axle was pronounced at the velocity of 25 and 15 kmph, respectively. The effect of an accelerating axle is noticeable when the axle moves at the velocities ranging from 0 to 30 kmph. In comparison to static load conditions, maximum % reduction in ε_{zz}, after reinforcement, was pronounced as high as 2.00 and 1.35 times larger for axle accelerating at 0.00 and 0.50 m/s^2.

6. Further Research

The weaknesses and limitations of the FE model developed in this study have indicated the following areas as recommendations for further work.

1. Further study based on advanced material models which can simulate the realistic behavior of subgrade, base, and geogrid can be done,
2. Further analysis of pavement response can be done by simulating the moving load with a specific contact area between tires and pavement surface, and
3. The pavement response in terms of stress-strain and deformation can be further analyzed by simulating the de-accelerating axle load on the pavement.

Acknowledgement

The authors would like to sincerely thank Er. Ashok Poudel for his critical comments and invaluable suggestions during the manuscript preparation of this research article.

References

[1] Nik Daud N. N., Jalil F. N.A., Celik S., and Albayrak Z. N.K. The important aspects of subgrade stabilization for road construction. 2019.

[2] Mathew Tom V. and Rao KV Krishna. *Introduction to Transportation Engineering*. NPTEL, 2007.

[3] Jorge G. Zornberg. Functions and applications of geosynthetics in roadways. 2017.

[4] Nader Ghafoori and Sharbaf M. *Use of geogrid for strengthening and reducing the roadway structural sections*. Nevada Department of Transportation, 2016.

[5] Wu Chaoyang, Wang Hao, Zhao Jingnan, Jiang Xin, Yanjun Qiu, and Bekhzad Yusupov. Prediction of viscoelastic pavement responses under moving load and nonuniform tire contact stresses using 2.5-d finite element method. 2020.

[6] Indian Road Congress. *Guidelines for the Design of Flexible Pavement (IRC:37-2018), Forth Revision*. Indian Road Congress, 2018.

[7] Correia N. S. and Zornberg Jorge G. Mechanical response of flexible pavements enhanced with geogrid-reinforced asphalt overlays. 2016.

[8] S. W. Perkins. *Numerical modelling of geosynthetic reinforced flexible pavements*. Montana Department of Transportation, 2001.

[9] Al-Qadi Imad L., Dessouky Samer H., Kwon Jayhyun, and Tutumluer Erol. Geogrid-reinforced low-volume flexible pavements: Pavement response and geogrid optimal location. 2012.

[10] Leng J. and Gabr Mohammed A. Transportation research record. 2002.

[11] Ling Hoe I. and Liu Zheng. Performance of geosynthetic-reinforced asphalt pavements. 2001.